

This is the accepted manuscript made available via CHORUS. The article has been published as:

## Understanding Reentrance in Frustrated Magnets: The Case of the math

$$\text{Er}_{2/3}\text{Sn}_2\text{O}_7$$
 Pyrochlore

D. R. Yahne, D. Pereira, L. D. C. Jaubert, L. D. Sanjeewa, M. Powell, J. W. Kolis, Guangyong Xu, M. Enjalran, M. J. P. Gingras, and K. A. Ross

Phys. Rev. Lett. **127**, 277206 — Published 30 December 2021

DOI: [10.1103/PhysRevLett.127.277206](https://doi.org/10.1103/PhysRevLett.127.277206)

# Understanding Reentrance in Frustrated Magnets: the Case of the $\text{Er}_2\text{Sn}_2\text{O}_7$ Pyrochlore

D. R. Yahne,<sup>1</sup> D. Pereira,<sup>2</sup> L. D. C. Jaubert,<sup>3</sup> L. D. Sanjeewa,<sup>4</sup> M. Powell,<sup>5</sup> J. W. Kolis,<sup>5</sup> Guangyong Xu,<sup>6</sup> M. Enjalran,<sup>7</sup> M. J. P. Gingras,<sup>2,8</sup> and K. A. Ross<sup>1,8</sup>

<sup>1</sup>Department of Physics, Colorado State University, 200 W. Lake St., Fort Collins, CO 80523-1875, USA

<sup>2</sup>Department of Physics and Astronomy, University of Waterloo, Waterloo, Ontario N2L 3G1, Canada

<sup>3</sup>CNRS, Université de Bordeaux, LOMA, UMR 5798, 33400 Talence, France

<sup>4</sup>Department of Materials Science and Engineering, University of Tennessee, Knoxville, TN 37996, USA

<sup>5</sup>Department of Chemistry, Clemson University, Clemson, South Carolina 29634-0973, USA

<sup>6</sup>NIST Center for Neutron Research, National Institute of Standards and Technology, Gaithersburg, Maryland 20899, USA

<sup>7</sup>Department of Physics, Southern Connecticut State University,  
501 Crescent Street, New Haven, Connecticut 06515-1355, USA

<sup>8</sup>CIFAR, MaRS Centre, West Tower 661 University Ave., Suite 505, Toronto, ON, M5G 1M1, Canada

(Dated: November 11, 2021)

Reentrance, the return of a system from an ordered phase to a previously encountered less-ordered one as a controlled parameter is continuously varied, is a recurring theme found in disparate physical systems, yet its microscopic cause is often not investigated thoroughly. Here, through detailed characterization and theoretical modeling, we uncover the microscopic mechanism behind reentrance in the strongly frustrated pyrochlore antiferromagnet  $\text{Er}_2\text{Sn}_2\text{O}_7$ . We use single crystal heat capacity measurements to expose that  $\text{Er}_2\text{Sn}_2\text{O}_7$  exhibits multiple instances of reentrance in its magnetic field  $B$  vs. temperature  $T$  phase diagram for magnetic fields along three cubic high symmetry directions. Through classical Monte Carlo simulations, mean field theory and classical linear spin-wave expansions, we argue that the origins of the multiple occurrences of reentrance observed in  $\text{Er}_2\text{Sn}_2\text{O}_7$  are linked to soft modes. These soft modes arise from phase competition and enhance thermal fluctuations, that entropically stabilize a specific ordered phase, resulting in an increased transition temperature for certain field values and thus the reentrant behavior. Our work represents a detailed examination into the mechanisms responsible for reentrance in a frustrated magnet and may serve as a template for the interpretation of reentrant phenomena in other physical systems.

PACS numbers:

Within the field of magnetism, frustration refers to a system's inability to simultaneously satisfy all of its energetic preferences. Strong frustration can result in a variety of exotic phenomena such as spin liquids, spin ice, emergent quasiparticles, topological phases and order-by-disorder [1–7]. Most of the research focus in this area over the past thirty years has been devoted to investigating the physics near zero temperature, considering finite temperatures as a necessary *modus operandi* to search for signatures of the low-energy properties. However, even when subject to high frustration, a majority of frustrated magnetic materials ultimately develop long-range order or display spin-glass freezing at a nonzero critical temperature  $T_c$ , albeit often at a very low one compared to the spin-spin interactions. In this context, it therefore seems natural to ask what behavior near  $T_c$  may be a witness of the zero-temperature ground state physics. This is particularly important when  $T_c$  is just above the experimental baseline temperature, so that temperatures which are low relative to  $T_c$  cannot be reached. Here we precisely consider such a situation, as arises in the  $\text{Er}_2\text{Sn}_2\text{O}_7$  pyrochlore antiferromagnet, and which provides an opportunity to study a recurrent aspect of frustrated magnetic systems observed at nonzero temperature: reentrance [8–16].

Reentrance occurs when a system, after having developed an ordered phase of some sort, returns to its original less-ordered (e.g. paramagnetic) state as some parameter (e.g. temperature, field, pressure, stoichiometry) is continuously varied. Reentrance has been found in spin glasses [17, 18],

liquid mixtures [19, 20], protein thermodynamics [21], liquid crystals [22, 23], bilayer graphene [24], superconductors [25], modulated phases [26, 27] and even in black hole thermodynamics [28]. Despite its ubiquity, reentrance is typically unexpected and its explanation in terms of entropic contributions to the free-energy from the underlying microscopic degrees of freedom is usually subtle. In this context, while frequently observed in frustrated magnets, the microscopic mechanism leading to reentrance often remains obscure [8–15]. Two mechanisms have commonly been invoked: a field-dependent suppression of quantum fluctuations [29–31] and the partial disorder of an intervening phase [18, 32–34]. Here, we present an alternative scenario of a generic nature which illustrates how the observation of reentrance may be used as a fingerprint of the frustration at play in the ground state.

In this article, we show that  $\text{Er}_2\text{Sn}_2\text{O}_7$  represents a tractable material example where the intricate microscopic mechanisms responsible for reentrance in frustrated magnets can be rigorously studied experimentally and theoretically.  $\text{Er}_2\text{Sn}_2\text{O}_7$  holds a special place among rare earth pyrochlores [5, 35]: it is well-characterized, has a suppressed critical temperature and is one of the few materials with a simple Palmer-Chalker (PC) antiferromagnetic ground state [36–38] [Fig. 1(a)]. Its estimated exchange and single-ion susceptibility parameters are highly anisotropic and theory suggests a proximity to another competing antiferromagnetic phase [37–39] known as  $\Gamma_5$  [5, 6, 39] [Fig. 1(b,c)]. Because of this anisotropy, the

response of  $\text{Er}_2\text{Sn}_2\text{O}_7$  to an applied field is expected to differ with field direction, as has been poignantly illustrated with the experimental exploration of rare earth pyrochlore titanates [5, 6, 11, 12, 35]. As such, the present study critically relies on the recently gained, and notoriously challenging, ability to synthesize pyrochlore stannate single crystals [40], including  $\text{Er}_2\text{Sn}_2\text{O}_7$ .

We report herein the discovery of five occurrences of reentrance in the  $B$ - $T$  phase diagram of  $\text{Er}_2\text{Sn}_2\text{O}_7$  for fields along the [100], [110] and [111] cubic directions using heat capacity measurements. By thoroughly investigating this experimental phase diagram using mean field theory, classical linear spin-wave expansions and Monte Carlo simulations, we have uncovered the various, and distinct, microscopic origins of reentrance in this system. In short, we find that multi-phase competitions at  $T = 0$  result in enhanced thermal fluctuations at specific field values. These fluctuations *entropically* stabilize the corresponding *ordered* phase over the disordered phase, and thus increase  $T_c(B)$  over a certain  $B$  field range. This produces  $T_c(B)$  reentrant phase boundaries whose maximal temperature extent corresponds approximately to the zero-temperature field-driven phase transitions [see Fig. 2(a-c)]. This multi-phase competition is in some cases a direct consequence of the competition of the field-evolved PC states while in others it is inherent to  $\text{Er}_2\text{Sn}_2\text{O}_7$ 's zero-field ground state being in close proximity to the phase boundary between the PC and  $\Gamma_5$  phases. See the Supplementary Material [45] for technical details on the experiments, simulations and analytics.

Heat capacity ( $C_p$ ) measurements were performed on single crystal samples, grown via the hydrothermal method described in Ref. [40], down to 50 mK with varying magnetic fields,  $B$ , oriented in the [111], [110], and [100] directions, using a dilution refrigerator insert in a Quantum Design Physical Properties Measurement System. Two measurement techniques were used: the conventional quasi-adiabatic thermal relaxation method (called "short pulses" hereafter), as well as "long pulses", both of which are described in detail in Ref. [49]. The long pulse technique allows faster and higher point-density measurements across phase transitions, enabling an accurate mapping of a phase diagram by measuring the field dependence of the transition temperature,  $T_c(B)$  [Fig. 1 (d)].

In the zero-field heat capacity [Fig. 1 (d) inset], we find a sharp lambda-like anomaly indicative of a phase transition at  $T_c = 118 \pm 5$  mK, which is consistent with previous measurements on powder samples reported in Ref. [48] (130 mK, from heat capacity, data shown in Fig. 1 (d) inset) and Ref. [38] ( $108 \pm 5$  mK, from DC magnetic susceptibility). The extremely high point density of the long pulse measurements allow for the observation of subtle features in the peak shape, which are typically not resolved by conventional short pulse measurements. This reveals a low temperature shoulder of the  $C_p$  peak in the zero-field data at  $97 \pm 5$  mK [45]. We performed elastic neutron scattering measurements to determine the magnetic structure between the sharp high

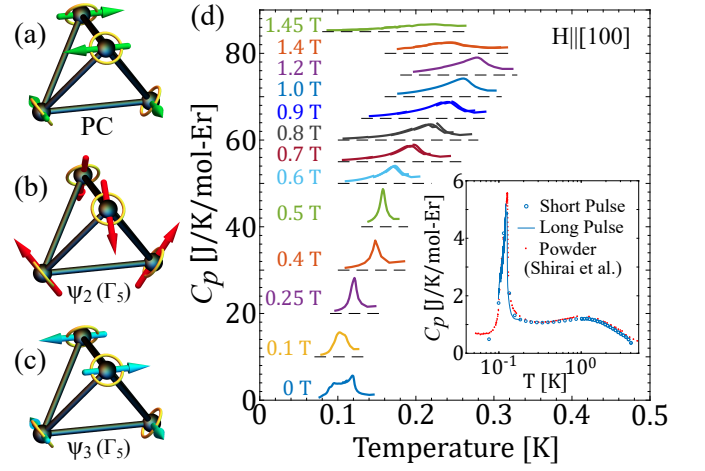


FIG. 1: Example of 6-fold degenerate states: (a) Palmer-Chalker [36] and (b)  $\psi_2$  and (c)  $\psi_3$  basis states of  $\Gamma_5$  [46]. The  $\psi_2$  and  $\psi_3$  states are connected by a rotation of the spins by an angle  $\phi$  within their local easy-planes (yellow circles):  $\phi \equiv n\pi/3$  ( $+\pi/6$ ) for  $n = 0, \dots, 5$  correspond to  $\psi_2$  ( $\psi_3$ ) [47]. Panels (b) and (c) are for  $\phi = 0$  and  $\pi/2$ , respectively. The manifold with U(1) degeneracy,  $\phi \in [0, 2\pi]$ , forms the so-called  $\Gamma_5$  states that appear in the [111] phase diagram. (d) Heat capacity,  $C_p(T)$ , vs temperature,  $T$ , of  $\text{Er}_2\text{Sn}_2\text{O}_7$  with the magnetic field along [100], showing the reentrant nature of the transition. Curves at different fields are offset vertically for clarity. Similar data for the [110] and [111] field directions are included in the Supplementary Material [45]. (Inset)  $C_p(T)$   $\text{Er}_2\text{Sn}_2\text{O}_7$  in zero-field, with short and long pulse measurements on crystal samples overlaid. Powder data from Shirai *et al.* [48] is also overlaid to demonstrate agreement between sample types.

temperature peak and the low temperature shoulder to check for an intermediate magnetic phase [45]. We found that the magnetic structure is of Palmer-Chalker type at all measured temperatures throughout the transition range with no sign of other magnetic phases. It is not clear what causes this structure in the heat capacity anomaly, but we note that similar (though not identical) broadening is observed in all five crystals we have measured as well as in published data on a powder sample [45, 48] (Fig. 1 (d) inset). Thus, it seems to be a feature of all  $\text{Er}_2\text{Sn}_2\text{O}_7$  samples, but is likely due to (or influenced by) slight inhomogeneities rather than being purely intrinsic in origin. Although it may be worth future investigation, its presence does not affect any of the conclusions of this work.

To model  $\text{Er}_2\text{Sn}_2\text{O}_7$ , we use the generic nearest-neighbor Hamiltonian on the pyrochlore lattice [39, 50],

$$\mathcal{H} = \sum_{\langle i,j \rangle} J_{ij}^{\alpha\beta} S_i^\alpha S_j^\beta - \mu_B \sum_i g_i^{\alpha\beta} B^\alpha S_i^\beta. \quad (1)$$

$S_i = (S_i^x, S_i^y, S_i^z)$  is a three-component pseudo-spin of length  $|S_i| = 1/2$  and  $B$  is the external magnetic field. The  $g$ -tensor represents the single-ion anisotropy, with local easy-plane  $g_\perp$  and easy-axis  $g_\parallel$  components at lattice site  $i$ . Given the symmetries of the pyrochlore lattice, the anisotropic exchange matrix  $J_{ij}^{\alpha\beta}$  is parameterized by four independent cou-

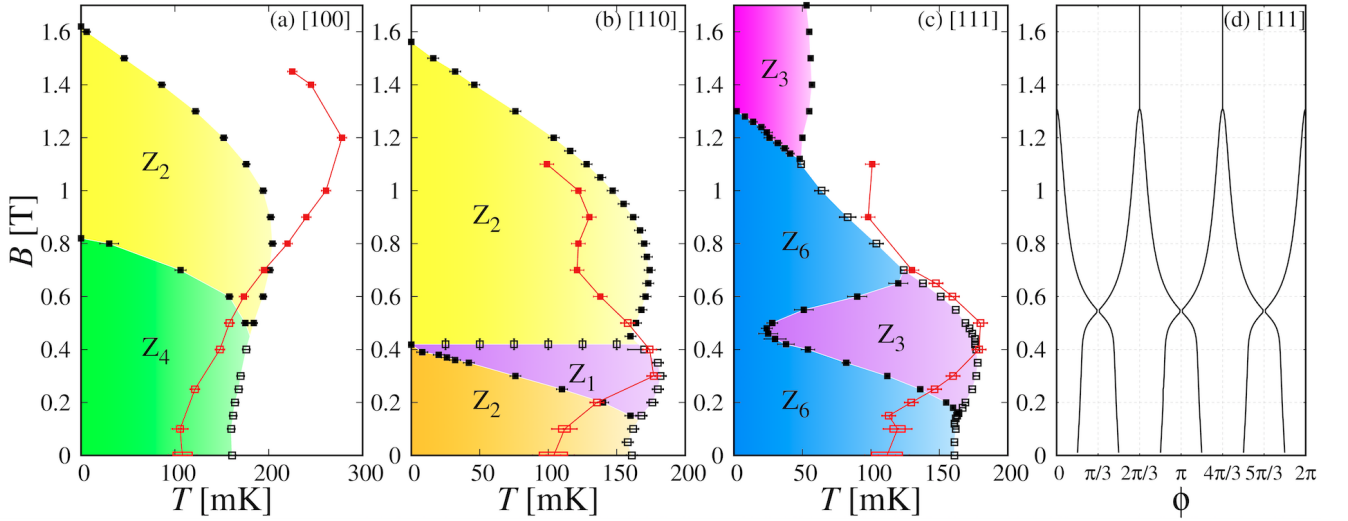


FIG. 2:  $B$ - $T$  phase diagrams of  $\text{Er}_2\text{Sn}_2\text{O}_7$  in the (a) [100], (b) [110] and (c) [111] field directions, comparing experimental data with sharp ( $\square$ ) and smooth ( $\blacksquare$ ) heat-capacity peaks [Fig. 1(d)], to Monte Carlo results with 1<sup>st</sup> ( $\square$ ) and 2<sup>nd</sup> ( $\blacksquare$ ) order transitions. Experiments and simulations are notably similar, showing the same (multiple) reentrance. The degeneracy  $Z_n$  found in simulations is given for each phase. The width of the red rectangles at 0 and 0.1 T represent the position of the double peaks. (d) In a [111] field, each of the six FEPC ground states has a  $\Gamma_5$  contribution described by an angle  $\phi$  [Fig. 1(b,c)], that can be computed exactly by minimizing the energy of one tetrahedron as a function of  $B$ .

pling constants:  $(J_1, J_2, J_3, J_4)$  [50, 51].  $\text{Er}_2\text{Sn}_2\text{O}_7$  has been previously parameterized using inelastic neutron scattering on powder samples [37, 38]. Here we choose to remain within the error bars of Ref. [38], selecting a set of coupling parameters where simulations find  $T_c \sim 180$  mK at 0.4 T for a [111] field to match the experimental result [61]:  $(J_1, J_2, J_3, J_4) = (+0.079, +0.066, -0.111, +0.032)$  meV and  $g_\perp = 7.52, g_\parallel = 0.054$ . Note that the nearest-neighbor part of dipolar interactions is included in the  $J_{ij}^{\alpha\beta}$  couplings of the Hamiltonian (1).

To proceed, we first analyze this model using classical Monte Carlo simulations, with the results summarized in the  $B$ - $T$  phase diagrams of Fig. 2. Most importantly, with  $T_c(B = 0.4 \text{ T})$  fitted (for  $B$  along the [111] direction), the simulations reproduce the number of reentrant “lobes” for each field direction (e.g. one and two for a [100] and [110] field, respectively), as well as, at each lobe, the rough magnitude of the increase of  $T_c$  at the corresponding value of  $B$ . Moreover, simulations find that the transition always evolves from discontinuous to continuous when increasing the field. This is consistent with the shape of the experimental heat capacity peaks, evolving from sharp to smooth, and a further hint that simulations are capturing the proper physics displayed by the experiments. We suspect that a fine-tuning of the  $J_{ij}^{\alpha\beta}$  coupling parameters and incorporating quantum fluctuations, as well as perhaps dipolar interactions beyond nearest neighbors, should account for the quantitative disagreements. Nevertheless, the semi-quantitative match between experiments and simulations confirms the validity of Eq. (1) as a minimal model for  $\text{Er}_2\text{Sn}_2\text{O}_7$ , suggesting that simulations robustly encapsulate the key physics behind the experimentally observed multiple occurrences of reentrance.

The results in Figs. 2(a-c) raise multiple questions. Why are there multiple instances of reentrance and why are they so strongly dependent on the field direction? More fundamentally, why does  $\text{Er}_2\text{Sn}_2\text{O}_7$  demonstrate reentrance in the first place? As a set of clues, simulations bring to light a variety of phases that vie for ordering. In the rest of this article, we explain how soft modes induced by this multi-phase competition are linked to reentrance, using a combination of mean field theory and classical linear spin-wave expansions.

The zero-field ground state of  $\text{Er}_2\text{Sn}_2\text{O}_7$  is the sixfold-degenerate PC phase. However, the ground states naturally deform and evolve under the application of a magnetic field. For sufficiently large fields, some of these field-evolved PC (FEPC) states may become partially polarized into the *same* spin configuration. We therefore label the resulting phase according to the number of FEPC states that minimize the free energy but have *distinct* spin configurations (e.g.  $Z_6$  at  $B = T = 0$ , for the six degenerate PC states, and  $Z_1$  at sufficiently large  $B$  for the trivial field-polarized paramagnet). Phase transitions then occur whenever distinct FEPC states “merge” into the same spin configuration at a given field value  $B_c$ .

First, consider the [100] field phase diagram in Fig. 2(a). At  $T = 0$ , the FEPC states merge at  $B_c = 0.82$  T, giving rise to the yellow  $Z_2$  region. Fig. 3 displays the classical spin-wave dispersions  $\kappa_\nu(\mathbf{q})$  for a number of field values below and above  $B_c$ , calculated from the corresponding  $T = 0$  FEPC ground states. As the merger transition is approached at  $B_c = 0.82$  T, the bottom of the dispersive bands drop below the energy scale set by  $T_c(B = 0) \approx 160$  mK, becoming soft and gapless at  $B = B_c$ . This decrease indicates a propensity for stronger thermal fluctuations at  $B_c$  than at other field values. More precisely, since  $s = -\frac{1}{8N_q} \sum_{\mathbf{q}} \sum_{\nu=1}^8 \ln(\kappa_\nu(\mathbf{q}))$  quantifies the



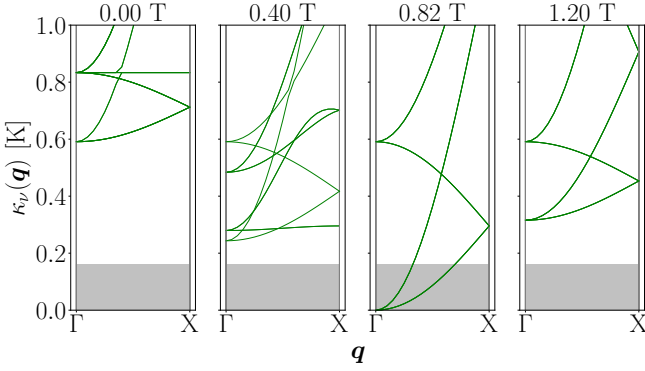


FIG. 3: Classical spin-wave dispersions for  $B = 0, 0.40, 0.82$ , and  $1.20$  T along the  $[100]$  direction, for a path in the FCC Brillouin zone. Note that  $B_c = 0.82$  T is a critical field at  $T = 0$ , as shown in Fig. 2. The grey boxes indicate energy scales below  $T_c(B = 0 \text{ T}) \approx 160$  mK from Monte Carlo simulations; when modes occur within this region they are considered “soft”. Note that the dispersions for *all* Palmer-Chalker states are plotted, but may overlap at high-symmetry points or due to their degeneracies in a field.

entropy contribution from classical spin-waves, the decrease in  $\kappa_v(q)$  on approaching  $B_c$  from above or below (as shown in Fig. 3) corresponds to an *increase* in entropy within the ordered phase. As a consequence, the gapless soft modes at  $B_c$  stabilize the yellow  $Z_2$  region of Fig. 2 at finite temperature, both over the green  $Z_4$  region as well as the disordered paramagnet.

At first sight, the above discussion may remind the reader of order-by-disorder, but the two mechanisms are in general different. Specifically, the  $Z_2$  selection for  $B \geq B_c$  is energetic and *not* entropic. As opposed to order-by-disorder, soft modes do not select the  $Z_2$  states among a degenerate manifold, but rather enhance their entropic stability at a specific field,  $B_c$ , compared to higher and lower fields. This pushes the transition temperature upwards around  $B_c$ , inducing reentrance.

The microscopic physics at play is different in a  $[111]$  field; simulations reveal a reentrant lobe around a field value ( $\sim 0.4$  T) for which no corresponding  $T = 0$  FEPC merger is found in the calculations. To understand this reentrance, it is important to note that the long-range order of  $\text{Er}_2\text{Sn}_2\text{O}_7$  in a  $[111]$  field is not described by a single irreducible representation (irrep) [39]. Instead, it is described by the naturally field-induced ferromagnetic irrep as well as the  $\Gamma_5$  irrep [Fig. 1(b,c)] due to the proximity of the  $\Gamma_5$  ground state to the PC phase in zero-field [39]. The  $\Gamma_5$  states bear an accidental  $U(1)$  degeneracy parameterized by an angle  $\phi$  [39, 47, 52–54], which is lifted by a magnetic field [55] with discrete values of  $\phi$  being selected, as shown in Fig. 2(d). While the six FEPC states remain distinct in this region, their  $\Gamma_5$  components merge at  $B \approx 0.55$  T into three  $\phi = \{\pi/3, \pi, 5\pi/3\}$  corresponding to three of the six  $\psi_2$  states [Fig. 1(b), Ref. [45]]. This  $\psi_2$  selection is associated with a flat low-energy soft mode in the spin-wave expansion at  $B \approx 0.5$  T and simulations confirm the presence of partial  $\psi_2$  order in the reentrant lobe, shown by the violet  $Z_3$  phase in Fig. 2(c). These results make a strong case unraveling

the mechanism of reentrance; the intervening  $Z_3$  phase, which is *not* part of the ground states, is entropically stabilized by low-energy soft modes arising from the PC and  $\Gamma_5(\psi_2)$  phase competition.

Closing the  $[111]$  case, one should mention the FEPC merger transition at  $B_c = 1.31$  T and  $T = 0$  is naturally accompanied by a merging of the  $\phi$  values (here also corresponding to  $\psi_2$  states, see Fig. 2(d)) and by a small reentrant lobe [Fig. 2(c)], as expected from the discussion for the  $[100]$  field case. Our experimental data point towards the onset of this high-field lobe as well (see Fig. 2(c) for  $B = 0.9$  T &  $1.1$  T). However, it was not possible to explore this high-field region experimentally because the sample did not easily equilibrate above  $0.7$  T. Interestingly, simulations also suffer from difficulties thermalizing between  $0.7$  and  $1.2$  T.

Finally, the mechanisms behind reentrance for a  $[110]$  field are reminiscent of the other two field directions [Fig. 2(b)]. Below  $B \lesssim 0.1$  T, simulations are difficult to thermalize [45], but above  $B \gtrsim 0.1$  T, we find two FEPC ground states that merge at  $B_c = 0.42$  T. This merging gives rise to gapless soft modes, the subsequent violet  $Z_1$  phase, and reentrance at finite temperatures. It is the same mechanism as in a  $[100]$  field. However, as opposed to the  $[100]$  scenario, this newly merged ground state vanishes immediately once  $B > B_c$  (i.e. it becomes an excited state). The system is then found in two *other* ground states (corresponding to the yellow  $Z_2$  phase). The vanishing of the merged state corresponds to the  $Z_1$  phase abruptly disappearing above  $B_c$  and the removal of the aforementioned gapless soft modes. This causes the rapid collapse of the reentrant lobe at  $B \sim 0.42$  T. The fact that  $Z_1$  order is only stable at one point at  $T = 0$  is reminiscent of the triangular Heisenberg antiferromagnet in a field, where an intervening  $1/3$  plateau also spreads at finite temperature and gives rise to reentrance [8, 13, 56] – a mechanism that might be at play in  $\text{Ba}_3\text{CoSb}_2\text{O}_9$  [57]. However, the reentrance phenomenon in our system at  $0.42$  T differs from this case in that it does not require the extensive degeneracy of a magnetization plateau, but simply the more generic presence of soft modes about a long-range ordered non-degenerate spin configuration.

At higher  $[110]$  field, another reentrant dome appears ( $B \sim 0.7$  T), however, there are no ground state FEPC mergers involved. Similarly to the reentrant behavior at low  $[111]$  field, spin wave theory shows a *minimum (non-zero) gap* that entropically favors the ordered phase around  $0.7$  T (see Section S5 in Ref [45]). These low-energy gapped modes, along with the collapse at  $B_c = 0.42$  T, give the higher field reentrant lobe at  $\sim 0.7$  T.

In summary, we have presented the first exploration of the field-direction dependence of the thermodynamics of stannate pyrochlores, which, despite decades of effort, were not available as single crystals until very recently [40]. Access to these crystals has proven to be crucial since the phase diagram of  $\text{Er}_2\text{Sn}_2\text{O}_7$  is highly sensitive to the field direction, and exhibits several reentrant lobes with sundry underlying mechanisms. These features result from the competition of several orders, especially the zero-field Palmer-Chalker, the field-induced fer-

romagnetic and the neighboring  $\Gamma_5$  states. In particular, most instances of reentrance in the phase diagram can be traced to zero-temperature field-induced merging of ground states. This energetic selection is accompanied by soft modes which entropically enhance the transition temperatures, and this mechanism is thus distinct from the one of order-by-disorder. In this light, reentrance is a useful and experimentally accessible fingerprint at the critical temperature of an underlying zero-temperature phase transition.

Given that multi-phase competition is a common feature of frustrated magnetism, we expect the mechanisms we have uncovered to be widespread among magnetic systems displaying reentrance; especially since it does not require the accidental presence of an exotic partially-disordered phase [18, 33, 58–60] or a phase with extensive entropy, such as in a magnetization plateau state [8, 13, 56, 57]. In semi-classical and quantum systems, our mechanism may work together with the field-induced suppression of quantum fluctuations [29] to produce even larger reentrant lobes. We hope our work will motivate others to pursue a microscopic interpretation of future observations of reentrance (and possibly to revisit old ones [8–16]) in light of zero-temperature transitions. Since magnetic systems often afford us with minimal models to understand other areas of physics, our results raise a more general question: if reentrance is observed by varying a given parameter, when is it actually due to a nearby transition in a broader, and perhaps not even physically accessible, parameter space?

We acknowledge Natalia Perkins for useful discussions and Rob Mann for comments on reentrance in black holes. We thank Allen Scheie and Tom Hogan for their help with analyzing the long pulse measurements, and acknowledge the use of the LongHCPulse program for this analysis. We thank I. Zivkovic and R. Freitas for providing us their  $C_p$  data previously published in Ref.[48]. We acknowledge the support of the National Institute of Standards and Technology, U.S. Department of Commerce, in providing the neutron research facilities used in this work. This research was partially supported by CIFAR. DRY, KAR, and JWK acknowledge funding from the Department of Energy award DE-SC0020071 during the preparation of this manuscript. The work at the University of Waterloo was supported by the Natural Sciences and Engineering Research Council (NSERC) and by the Canada Research Chairs Program (M.G, Tier 1). L. J. acknowledges financial support from CNRS (PICS No. 228338) and from the French “Agence Nationale de la Recherche” under Grant No. ANR-18-CE30-0011-01.

- 
- [1] L. Balents, "Spin liquids in frustrated magnets," *Nature* **464**, 199 (2010).
  - [2] M. J. P. Gingras and P. A. McClarty, "Quantum spin ice: a search for gapless quantum spin liquids in pyrochlore magnets," *Rep. Prog. Phys.* **77**, 056501 (2014).

- [3] L. Savary and L. Balents, "Quantum spin liquids: a review," *Rep. Prog. Phys.* **80**, 016502 (2017).
- [4] M. Hermanns, I. Kimchi, and J. Knolle, "Physics of the Kitaev model: Fractionalization, dynamic correlations, and material connections," *Annu. Rev. Condens. Matter Phys.* **9**, 17 (2018).
- [5] A. M. Hallas, J. Gaudet, and B. D. Gaulin, "Experimental insights into ground-state selection of quantum  $XY$  pyrochlores," *Annu. Rev. Condens. Matter Phys.* **9**, 105 (2018).
- [6] J. G. Rau and M. J. Gingras, "Frustrated Quantum Rare-Earth Pyrochlores," *Annu. Rev. Condens. Matter Phys.* **10**, 357 (2019).
- [7] J. Knolle and R. Moessner, "A field guide to spin liquids," *Annu. Rev. Condens. Matter Phys.* **10**, 451 (2019).
- [8] M. V. Gvozdkova, P.-E. Melchy, and M. E. Zhitomirsky, "Magnetic phase diagrams of classical triangular and kagomé antiferromagnets," *J. Phys. Condens. Matter* **23**, 164209 (2011).
- [9] R. Rawl, M. Lee, E. S. Choi, G. Li, K. W. Chen, R. Baumbach, C. R. Dela Cruz, J. Ma, and H. D. Zhou, "Magnetic properties of the triangular lattice magnets  $A_4B'B_2O_{12}$  ( $A = \text{Ba, Sr, La; } B' = \text{Co, Ni, Mn; } B = \text{W, Re}$ )," *Phys. Rev. B* **95**, 174438 (2017).
- [10] A. Scheie, J. Kindervater, S. Säubert, C. Duvinage, C. Pfleiderer, H. J. Changlani, S. Zhang, L. Harriger, K. Arpino, S. M. Koohpayeh, O. Tchernyshyov, and C. Broholm, "Reentrant phase diagram of  $\text{Yb}_2\text{Ti}_2\text{O}_7$  in a  $\langle 111 \rangle$  magnetic field," *Phys. Rev. Lett.* **119**, 127201 (2017).
- [11] S. Säubert, A. Scheie, C. Duvinage, J. Kindervater, S. Zhang, H. J. Changlani, G. Xu, S. M. Koohpayeh, O. Tchernyshyov, C. L. Broholm, and C. Pfleiderer, "Orientation dependence of the magnetic phase diagram of  $\text{Yb}_2\text{Ti}_2\text{O}_7$ ," *Phys. Rev. B* **101**, 174434 (2020).
- [12] O. A. Petrenko, M. R. Lees, G. Balakrishnan, and D. M. Paul, "Magnetic phase diagram of the antiferromagnetic pyrochlore  $\text{Gd}_2\text{Ti}_2\text{O}_7$ ," *Phys. Rev. B* **70**, 012402 (2004).
- [13] L. Seabra, T. Momoi, P. Sindzingre, and N. Shannon, "Phase diagram of the classical Heisenberg antiferromagnet on a triangular lattice in an applied magnetic field," *Phys. Rev. B* **84**, 214418 (2011).
- [14] L. Seabra, P. Sindzingre, T. Momoi, and N. Shannon, "Novel phases in a square-lattice frustrated ferromagnet :  $\frac{1}{3}$ -magnetization plateau, helicoidal spin liquid, and vortex crystal," *Phys. Rev. B* **93**, 085132 (2016).
- [15] M. Li, I. Rousochatzakis, and N. B. Perkins, "Reentrant incommensurate order and anomalous magnetic torque in the Kitaev magnet  $\beta\text{-Li}_2\text{IrO}_3$ ," *Phys. Rev. Res.* **2**, 033328 (2020).
- [16] A. Rousseau, J. M. Parent, and J. A. Quilliam, "Anisotropic phase diagram and spin fluctuations of the hyperkagome magnet  $\text{Gd}_3\text{Ga}_5\text{O}_{12}$  as revealed by sound velocity measurements," *Phys. Rev. B* **96**, 060411(R) (2017).
- [17] M. J. P. Gingras and E. S. Sørensen, "Evidence for a genuine ferromagnetic to paramagnetic reentrant phase transition in a Potts spin-glass model," *Phys. Rev. B* **57**, 10264 (1998).
- [18] H. T. Diep, *Magnetic Systems with Competing Interactions (Frustrated Spin Systems)* (World Scientific Publishing, 1994).
- [19] C. A. Vause and J. S. Walker, "Reappearing Phases," *Sci. Am.* **256**, 98 (1987).
- [20] C. A. Vause and J. S. Walker, "Effects of orientational degrees of freedom in closed-loop solubility phase diagrams," *Phys. Lett. A* **90**, 419 (1982), ISSN 0375-9601.
- [21] C. L. Dias, T. Ala-Nissila, J. Wong-ekkabut, I. Vattulainen, M. Grant, and M. Karttunen, "The hydrophobic effect and its role in cold denaturation," *Cryobiology* **60**, 91 (2010).
- [22] S. Singh, "Reentrant phase transitions in liquid crystals," *Phase Transit.* **72**, 183 (2000).

- [23] A. N. Berker and J. S. Walker, "Frustrated spin-gas model for doubly reentrant liquid crystals," *Phys. Rev. Lett.* **47**, 1469 (1981).
- [24] I. V. Lebedeva and A. M. Popov, "Two phases with different domain wall networks and a reentrant phase transition in bilayer graphene under strain," *Phys. Rev. Lett.* **124**, 116101 (2020).
- [25] T. H. Lin, X. Y. Shao, M. K. Wu, P. H. Hor, X. C. Jin, C. W. Chu, N. Evans, and R. Bayuzick, "Observation of a reentrant superconducting resistive transition in granular  $\text{BaPb}_{0.75}\text{Bi}_{0.25}\text{O}_3$  superconductor," *Phys. Rev. B* **29**, 1493 (1984).
- [26] A. Mendoza-Coto, L. Nicolao, and R. Díaz-Méndez, "On the mechanism behind the inverse melting in systems with competing interactions," *Sci. Rep.* **9**, 2020 (2019), ISSN 2045-2322.
- [27] A. Mendoza-Coto, D. E. B. de Oliveira, L. Nicolao, and R. Díaz-Méndez, "Topological phase diagrams of the frustrated Ising ferromagnet," *Phys. Rev. B* **101**, 174438 (2020).
- [28] N. Altamirano, D. Kubizňák, and R. B. Mann, "Reentrant phase transitions in rotating anti-de Sitter black holes," *Phys. Rev. D* **88**, 101502(R) (2013).
- [29] B. Schmidt and P. Thalmeier, "Néel temperature and reentrant  $H-T$  phase diagram of quasi-two-dimensional frustrated magnets," *Phys. Rev. B* **96**, 214443 (2017).
- [30] M. Skoulatos, F. Rucker, G. J. Nilsen, A. Bertin, E. Pomjakushina, J. Ollivier, A. Schneidewind, R. Georgii, O. Zaharko, L. Keller, et al., "Putative spin-nematic phase in  $\text{BaCdVO}(\text{PO}_4)_2$ ," *Phys. Rev. B* **100**, 014405 (2019).
- [31] K. M. Ranjith, S. Luther, T. Reimann, B. Schmidt, P. Schlender, J. Sichelschmidt, H. Yasuoka, A. M. Strydom, Y. Skourski, J. Wosnitza, H. Kuhne, T. Doert, and M. Baenitz, "Anisotropic field-induced ordering in the triangular-lattice quantum spin liquid  $\text{NaYbSe}_2$ ," *Phys. Rev. B* **100**, 224417 (2019).
- [32] V. Vaks, A. Larkin, and Y. N. Ovchinnikov, "Ising model with interaction between nonnearest neighbors," *Soviet Physics JETP* **22**, 820 (1966).
- [33] P. Azaria, H. T. Diep, and H. Giacomini, "Coexistence of order and disorder and reentrance in an exactly solvable model," *Phys. Rev. Lett.* **59**, 1629 (1987).
- [34] E. H. Boubcheur, R. Quartu, H. T. Diep, and O. Nagai, "Non-collinear XY spin system: First-order transition and evidence of a reentrance," *Phys. Rev. B* **58**, 400 (1998).
- [35] J. S. Gardner, M. J. P. Gingras, and J. E. Greedan, "Magnetic pyrochlore oxides," *Rev. Mod. Phys.* **82**, 53 (2010).
- [36] S. E. Palmer and J. T. Chalker, "Order induced by dipolar interactions in a geometrically frustrated antiferromagnet," *Phys. Rev. B* **62**, 488 (2000).
- [37] S. Guitteny, S. Petit, E. Lhotel, J. Robert, P. Bonville, A. Forget, and I. Mirebeau, "Palmer-Chalker correlations in the XY pyrochlore antiferromagnet  $\text{Er}_2\text{Sn}_2\text{O}_7$ ," *Phys. Rev. B* **88**, 134408 (2013).
- [38] S. Petit, E. Lhotel, F. Damay, P. Boutrouille, A. Forget, and D. Colson, "Long-range order in the dipolar antiferromagnet  $\text{Er}_2\text{Sn}_2\text{O}_7$ ," *Phys. Rev. Lett.* **119**, 187202 (2017).
- [39] H. Yan, O. Benton, L. Jaubert, and N. Shannon, "Theory of multiple-phase competition in pyrochlore magnets with anisotropic exchange with application to  $\text{Yb}_2\text{Ti}_2\text{O}_7$ ,  $\text{Er}_2\text{Ti}_2\text{O}_7$ , and  $\text{Er}_2\text{Sn}_2\text{O}_7$ ," *Phys. Rev. B* **95**, 094422 (2017).
- [40] M. Powell, L. D. Sanjeewa, C. D. McMillen, K. A. Ross, C. L. Sarkis, and J. W. Kolis, "Hydrothermal crystal growth of rare earth tin cubic pyrochlores,  $\text{RE}_2\text{Sn}_2\text{O}_7$  (RE = La-Lu): site ordered, low defect single crystals," *Cryst. Growth Des.* **19**, 4920 (2019).
- [41] J. N. Reimers, A. J. Berlinsky, and A.-C. Shi, "Mean-field approach to magnetic ordering in highly frustrated pyrochlores," *Phys. Rev. B* **43**, 865 (1991).
- [42] M. Enjalran and M. J. P. Gingras, "Theory of paramagnetic scattering in highly frustrated magnets with long-range dipole-dipole interactions: The case of the  $\text{Tb}_2\text{Ti}_2\text{O}_7$  pyrochlore antiferromagnet," *Phys. Rev. B* **70**, 174426 (2004).
- [43] M. Enjalran, A. Del Maestro, and M. J. P. Gingras, "Mean-Field theory of the soft mode spectrum and field-driven transitions in a dipolar Heisenberg pyrochlore antiferromagnet model," *unpublished*.
- [44] P. P. Ewald, "Die Berechnung optischer und elektrostatischer Gitterpotentiale," *Ann. Phys. (Leipzig)* **64**, 253 (1921)
- [45] See Supplemental Materials for additional technical details and which also includes Refs. [41–44].
- [46] A. Poole and A. S. Wills and E. Lelièvre-Berna, "Magnetic ordering in the XY pyrochlore antiferromagnet  $\text{Er}_2\text{Ti}_2\text{O}_7$ : a spherical neutron polarimetry study," *J. Phys. Condens. Matter* **19**, 452201 (2007).
- [47] L. Savary, K. A. Ross, B. D. Gaulin, J. P. C. Ruff, and L. Balents, "Order by quantum disorder in  $\text{Er}_2\text{Ti}_2\text{O}_7$ ," *Phys. Rev. Lett.* **109**, 167201 (2012).
- [48] M. Shirai, R. S. Freitas, J. Lago, S. T. Bramwell, C. Ritter, and I. Živković, "Doping-induced quantum crossover in  $\text{Er}_2\text{Ti}_{2-x}\text{Sn}_x\text{O}_7$ ," *Phys. Rev. B* **96**, 180411(R) (2017).
- [49] A. Scheie, "LongHCPulse: Long-pulse heat capacity on a Quantum Design PPMS," *J. Low Temp. Phys.* **193**, 60 (2018).
- [50] K. A. Ross, L. Savary, B. D. Gaulin, and L. Balents, "Quantum excitations in quantum spin ice," *Phys. Rev. X* **1**, 021002 (2011).
- [51] S. H. Curnoe, "Quantum spin configurations in  $\text{Tb}_2\text{Ti}_2\text{O}_7$ ," *Phys. Rev. B* **75**, 212404 (2007).
- [52] J. D. M. Champion, M. J. Harris, P. C. W. Holdsworth, A. S. Wills, G. Balakrishnan, S. T. Bramwell, E. Čížmár, T. Fennell, J. S. Gardner, J. Lago, D. F. McMorrow, M. Orendac, A. Orendacova, D. McK. Paul, R. I. Smith, M. T. F. Telling, and A. Wildes, " $\text{Er}_2\text{Ti}_2\text{O}_7$ : Evidence of quantum order by disorder in a frustrated antiferromagnet," *Phys. Rev. B* **68**, 020401(R) (2003).
- [53] M. E. Zhitomirsky, M. V. Gvozdikova, P. C. W. Holdsworth, and R. Moessner, "Quantum order by disorder and accidental soft mode in  $\text{Er}_2\text{Ti}_2\text{O}_7$ ," *Phys. Rev. Lett.* **109**, 077204 (2012).
- [54] J. Oitmaa, R. R. P. Singh, B. Javanparast, A. G. R. Day, B. V. Bagheri, and M. J. P. Gingras, "Phase transition and thermal order-by-disorder in the pyrochlore antiferromagnet  $\text{Er}_2\text{Ti}_2\text{O}_7$ : A high-temperature series expansion study," *Phys. Rev. B* **88**, 220404(R) (2013).
- [55] V. S. Maryasin, M. E. Zhitomirsky, and R. Moessner, "Low-field behavior of an XY pyrochlore antiferromagnet: Emergent clock anisotropies," *Phys. Rev. B* **93**, 100406(R) (2016).
- [56] S. Miyashita, "Phase transition in spin systems with various types of fluctuations," *Proceedings of the Japan Academy, Series B* **86**, 643–666 (2010).
- [57] A. Sera, Y. Kousaka, J. Akimitsu, M. Sera, T. Kawamata, Y. Koike, and K. Inoue, " $S = 1/2$  triangular-lattice antiferromagnets  $\text{Ba}_3\text{CoSb}_2\text{O}_9$  and  $\text{CsCuCl}_3$ : Role of spin-orbit coupling, crystalline electric field effect, and Dzyaloshinskii-Moriya interaction," *Phys. Rev. B* **94**, 214408 (2016).
- [58] U. F. P. Seifert, and M. Vojta, "Theory of partial quantum disorder in the stuffed honeycomb heisenberg antiferromagnet," *Phys. Rev. B* **99**, 155156 (2019).
- [59] M. G. Gonzalez, F. T. Lisandrini, G. G. Blesio, A. E. Trumper, C. J. Gazza, and L. O. Manuel, "Correlated partial disorder in a weakly frustrated quantum antiferromagnet," *Phys. Rev. Lett.* **122**, 017201 (2019).
- [60] Y. Yang, S. J. Ran, X. Chen, Z. Z. Sun, S. S. Gong, Z. Wang, and G. Su, "Reentrance of the topological phase in a spin-1 frustrated heisenberg chain," *Phys. Rev. B* **101**, 045133 (2020).

[61] Now that single crystals are available, fine-tuning these parameters by exploring the entire  $Q$ -space with neutron scattering would be a worthwhile endeavor for future work, albeit challeng-

ing due to the small mass of each crystal.